Evaluation of the Strength of Thin Metallic Films Coated on Brittle Materials by using an Indentation Fracture Method

Yuzo Nakamura [1], Takashi Kawabata [2, 3], Shinya Ishigami [2, 4]
Jun Wakiyama [1], Yoshikazu Maeda [1]

[1] Department of Mechanical Engineering, Graduate School of Science and Engineering
[2] Department of Nanostructure Advanced Materials, Graduate School of Engineering, Kagoshima University, Kagoshima 890-0065, Japan
[3] Present address: Kobe Mashinery Center, Kobe Steel Ltd., Takasago 676-8670, Japan
[4] Present address: NIDEC Co., Kyoto 601-8205, Japan
* Corresponding author: nakamura@mech.kagoshima-u.ac.jp

Abstract Nanoindentation techniques are poplar methods which are used for the evaluation of the hardness and elastic modulus of very thin films. However, since the plastic and elastic regions formed underneath the indenter are much larger than its penetration depth, the thickness of films, which can be used for the nanoindentation measurement, is limited to a certain value. In the present study, microcracking caused by micro-Vickers indentation was applied to the evaluation of the tensile properties of very thin metallic films coated on brittle materials. For this purpose, gold films with the thicknesses ranging from 23 nm to 227 nm were coated on glass substrates, and the lengths of radial cracks before and after coating were measured. The crack opening displacements in uncoated glass were also measured to assess the stress intensity factor at crack tips. In the case of 34 nm thick gold film, a fracture mechanics analysis based upon the crack-tip stress intensity factor led to the yield strength of about 620 MPa and the fracture toughness of 2.0 MPa·m$^{1/2}$. The evaluation of mechanical properties of thicker films, however, became more difficult, since the elongation in thicker films are considered to become comparable with the crack opening displacement.

Keywords Thin film, Indentation fracture, Mechanical properties, Stress intensity factor, crack opening displacement

1. Introduction

The Young's modulus, yield strength, ultimate tensile strength, work hardening exponent, elongation to failure and fracture toughness, are key factors which should be measured in order to guarantee the structural integrity of metallic materials. It is well known that the hardness can be related with the tensile properties of metals [1, 2]. According to contact mechanics, especially the analysis of Love [3] given for the elastic contact of a conical indenter with a semi-infinite body, the Young's modulus of the body can be estimated from the relation of the load with the contact area. This situation is realized by measuring the load-depth curve of elastic recovery which occurs during the unloading of indentation testing. Following this principle, a nanoindetation technique using the Berkovich indenter with a sharp apex has been developed currently, since a systematic study of Oliver and Pharr [4]. Nanoindentation shows its great applicability, in measuring the hardness and elastic modulus of very thin films to which normal tensile tests or hardness tests cannot be applied.
Hill [5] proposed a cavity theory, which treats the elastic-plastic stress problem around an internally pressurized cavity in an infinite body. The cavity theory has also been shown to be applicable in the analysis of the elastic-plastic stress fields around indent. According to Johnson [6], the radius, b, of plastic zone formed underneath a conical indenter with a half apex angle of ψ_c is given by

$$b = a[E\cot\psi_c/\{6(1-\nu)\sigma_y\} + 2(1-\nu)/\{3(1-2\nu)\}]^{1/3}, \quad (1)$$

where a is the radius of contact area, and E, ν and σ_y are is the Young's modulus, the Poisson's ratio and the yield strength, respectively. As for a conical indenter having the same projected hardness H and penetration depth h as those of the Vickers indenter, ψ_c becomes 70.3° and the radius of contact area is given by $a \approx 2.8h$. When $\nu = 0.3$, thus, equation (1) gives the value of b/h ranging from 2.8

to 26 for the change of E/σ_y from 100 (ultrahigh strength steels) to 10000 (annealed metals). Nearly the same values are obtained for b/h of the Berkovich indenter. One can see from this simple estimation that the penetration depth of the indenter, should be smaller by a factor of about 30 than the thickness of film, when its mechanical properties are not known. It should be also noted that, even if this requirement is satisfied, the elastic deformation of substrates on which the films are coated influences the penetrating behavior of indenter, leading to the change of measured hardness with penetration depth, as is demonstrated by Han *et al* [7]. On the other hand, as the load is lowered, the deformation mechanism underneath the indenter changes from the one representing the bulk properties to the one reflecting the generation of dislocations and their development to surrounding. Dietiker *et al*. [8] have shown that the critical penetration depth where this transition occurs is about 10 nm in single-crystalline Au films coated on NaCl substrates, when the Berkovich indenter is used. Accordingly the interpretation of hardness measured by nanoindentation becomes more complicated in thinner films than 200 nm. In addition to these problems, since the films are compressed by indentation, there is the possibility that the measured hardness does not represent their tensile properties, which are strongly affected by defects like small cavities introduced during synthesis.

It is well known that when an indenter is impressed on the surface of a ceramic material, cracks are formed around the indent at loads higher than a critical load [9]. Among such cracks, radial cracks with a half-penny shape formed by the Vickers indentation are frequently used to measure the fracture toughness of ceramic materials. The crack opening displacement (COD), δ_{tip}, very close to the tip of a radial crack with a radius of C can be approximately expressed as

$$\delta_{tip} \approx \delta_o \sqrt{\frac{2x}{C}} \text{ , where } \delta_o = \frac{4(1-\nu^2)K_{tip}\sqrt{C}}{\sqrt{\pi}E}, \tag{2}$$

which will be mentioned later. Here x is the distance from the crack tip toward the interior of crack and K_{tip} is the stress intensity factor (SIF) at the crack tip. Eq. (2) can be easily verified to hold true for any stress state acting on a circular crack in an infinite body. However the COD profile given by this equation deviates considerably from the one which is measured at distance far from the crack tip. Fett [10] proposed a sophisticated model of COD profile for the Vickers indentation crack by computer calculation, while Burghard *et al*. [11] used a polynominal equation of $x^{1/2}$ to fit it to the measured COD profiles. When we introduce a radial crack in a brittle substrate coated with very thin film of ductile metal, it is expected that the film be elongated at the crack mouth emerging at the film/substrate interface. The elongation changes with the COD along the crack, and its magnitude is considered related with the COD profile of the substrate. Despite that this microscopic elongation test by means of microcracking is dynamical and localized, we can obtain the information on the tensile properties of the film.

In the present study, microcracking by means of the Vickers indentation is used as a nanoscale tensile testing of thin metallic films coated on brittle substrates, and a fracture mechanics model to estimate the tensile properties of the films is proposed. In order to check the validity of the model, gold film and glass substrate are used as a model film/substrate system. The Young's moduli of these materials are nearly equal so that we can ignore the misfit in elastic behavior between the film and substrate. The Vickers indentation cracks are introduced in Au film/glass substrate systems (hereafter called Au/glass) by varying the film thickness and changing the indentation load. The indent size, crack size and COD profile in uncoated glass as well as in Au/glass are measured, and the yield strength, plastic work and fracture toughness of Au films are evaluated based upon the proposed model.

2. Modeling

2.1 SIF and COD

Lawn *et al.* [11, 12] showed, by using glass, that small circular cracks were first formed underneath the Vickers indenter during loading, and then the cracks grew into semi-circular ones during unloading. Thus the driving force for the development of the radial cracks, observed after the Vickers indentation, is substantially provided by the residual pressure remaining in the plastic zone formed underneath the indent. Assuming that the stress field around the plastic zone is represented by the cavity theory [5, 6], the circumferential stress around the plastic zone is given by

$$\sigma_\theta = p_r b^3/2r^3, \tag{3}$$

Here r is the distance from the center of indent and p_r is the residual pressure within the plastic zone. The stress intensity factor (SIF) of the radial crack with a radius C is then expressed as

$$K = \frac{2\alpha Y_s Y_c}{\sqrt{\pi C}} \int_b^C \frac{\sigma_\theta r dr}{\sqrt{C^2 - r^2}}, \tag{4}$$

by applying the SIF given for a circular crack in an infinite body [13]. Here the coefficients, Y_s and Y_c, are correction factors arising from the effects of surface and crack interaction, respectively, and α is a correction factor, which modifies the deviation from the assumed cavity theory as well as the assumed half-penny shape of radial cracks. By inserting Eq. (3) into Eq. (4) and integrating it, one can obtain the following formula.

$$K = \chi P / C^{3/2} \sqrt{1 - (b/C)^2}, \tag{5}$$

where P is the indentation load and χ is a parameter that correlates the SIF due to load P with that of stress σ_θ. , *i.e.*, $\chi = \alpha Y_s Y_c p_r b^2/\pi^{1/2}/P$. It should be noted here that this equation does not involve the pressure within the plastic zone, which acts as the force to close the crack in the zone [10]. When the crack is larger by a factor of more than three than the plastic zone, *i.e.*, $C \geq 3b$, $\{1-(b/C)^2\}^{1/2} \approx 1$ so that the above equation is approximately written as

$$K = \chi P / C^{3/2}. \tag{6}$$

The condition $C >> b$ also enables us to ignore the closing effect of pressure within the plastic zone. There have been many formulae that relate χ with the properties of materials and the characteristics of indent [13]. In the present analysis, we use the formula, $\chi = 0.016(E/H)^{1/2}$, which was proposed by Anstis *et al.* [14]. Here the projected hardness is defined by $H = 2P/d^2$, where d is the diagonal length of Vickers indent.

The COD at a distance of r from the center of indent is given by [15]

$$\delta(r) = \frac{4(1-\nu^2)}{\sqrt{\pi} E} \int_r^C \frac{\sqrt{C'} K(C') dC'}{\sqrt{C'^2 - r^2}}. \tag{7}$$

The insertion of Eq. (6) into Eq. (7) and the use of the formula of integral [16] lead to

$$\delta(r) = \delta_o \frac{\arccos(r/C)}{r/C}. \tag{8}$$

This equation does not cover the COD profile over the whole crack length. However, it reproduces the COD profile at longer distances from the crack tip than Eq. (2) does. Thus Eq. (8) is satisfactory and its simple form is very useful in the present analysis of COD, as will be mentioned below. One can also see that Eq. (7) approaches Eq. (2) irrespectively of the form of K, when $x << C$.

2.2 Evaluation of yield strength of metallic films

When a ductile film deposited on a brittle substrate does not have large enough strength to close the crack mouth in the substrate, the film is considered to be elongated at the crack mouth, as is shown in Fig. 1. Since the film thickness, t_o, considered here is much smaller than the radial crack size, it is assumed that the film is elongated only at the crack mouth. It is anticipated that the film fails, when the COD exceeds the elongation to failure of the film which is isolated from the substrate. Hence the half crack length C_f observed at the surface of film/substrate system is expected to be smaller

than the half crack length C of uncoated substrate. It is also postulated that the plastic work done until the failure of the film is much larger than the surface energy of the film so that we can ignore the term related with the surface energy. Assuming that the film is a rigid-plastic body having the yield strength of σ_y, the plastic work done in an element between x an $x + dx$ is given by

$$dW_p = \sigma_y \int_0^{\delta} t dx d\delta , \tag{9}$$

where t is the thickness at the distance of x. The film thickness changes with δ. Assuming that plastic deformation in the film is constrained at the film/substrate surface, it is considered that the shear displacement through thickness takes place at the angles of ±45° from the surface, as shown in Fig. 2, following the maximum shear stress theory [5]. The geometrical condition of this constraint deformation leads to

$$t(\delta) = -\delta/2 + \sqrt{\delta^2/4 + {t_o}^2} . \tag{10}$$

Consequently the plastic work done in the plastic zone of the film becomes

$$W_p = \sigma_y V(R) , \tag{11}$$

where $V(R)$ implies the volume of plastic zone and is given by

$$V(R) = \int_0^R \int_0^{\delta} t(\delta) d\delta dx . \tag{12}$$

Here R is the distance of plastic zone in the film and is given by the difference in half crack size between the substrate and film, *i.e.*, $R = C - C_f$. The integration of $t(\delta)$ with regard to δ in the above equation leads to

$$T(\delta) = \int_0^{\delta} t(\delta) d\delta = \frac{\delta\sqrt{\delta^2 + 4{t_o}^2} - \delta^2}{4} + {t_o}^2 \ln\left[\tan\left(\frac{\pi}{4} + \frac{1}{2} \arctan\frac{\delta}{2t_o} \right) \right]. \tag{13}$$

On the other hand, the film/substrate system increases its fracture toughness due to the reduction in crack size. Assuming that the SIF in the film is expressed by Eq. (6), the elastic energy in the film,

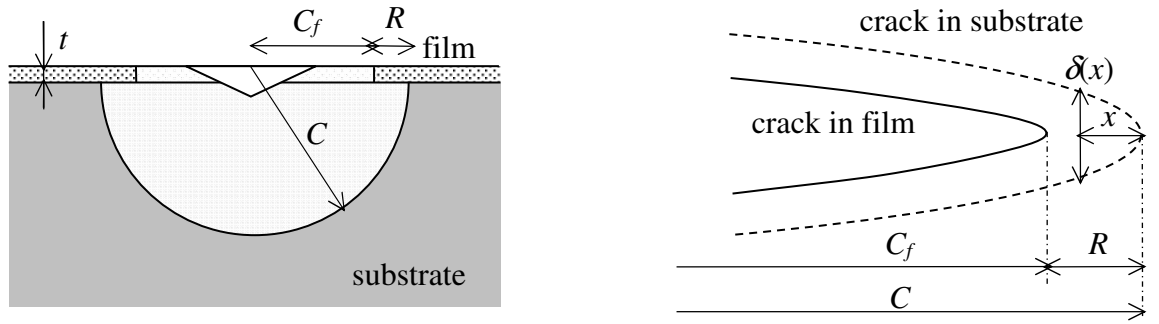

(a) Cross-sectional view. (b) Top view near crack tip.

Fig. 1. Film/substrate crack in which the crack tip is discontinuous at the film/substrate interface.

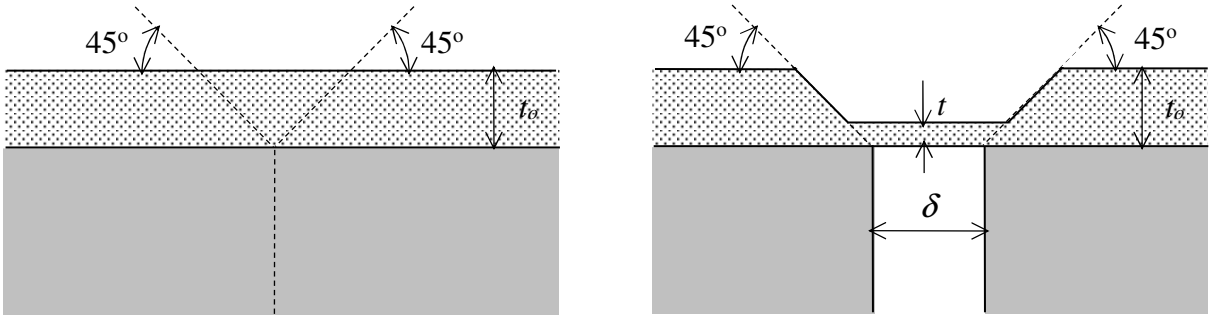

(a) Before cracking. (b) After cracking.

Fig. 2. Assumed mechanism of plastic deformation in film.

which is required to reduce the crack size from C to Cf, is written as follows.

$$U_e = \int_{C_f}^{C} \frac{K(C')^2}{E_f} t_o dC' = \frac{K_C{}^2 t_o}{2E_f} \frac{CR(2C-R)}{(C-R)^2}. \quad (14)$$

where E_f is the Young's modulus of the film. By equating U_e with W_p, the yield strength of the film is given by

$$\sigma_y = \frac{K_C{}^2}{E_f t_o} \frac{CR(2C-R)}{V(R)(C-R)^2}. \quad (15)$$

Since the elongation of the film increases with increasing the distance from crack tip in the substrate, the plastic work per unit area consumed in the plastic zone of the film is also expected to increase with distance from the crack tip in the substrate. Accordingly the local plastic work per unit area can be defined as follows.

$$\gamma_p(x) = \frac{dW_p}{t(x)dx} = \frac{\sigma_y T(\delta)}{t(\delta)}. \quad (16)$$

We can evaluate the profile of local plastic work as a function of x by using the dependence of δ on x. The maximum value of local plastic work is obtained at $x = R$, which corresponds to the plastic work done to failure. Accordingly the fracture toughness of the film is given by

$$K_{fC} = \sqrt{E_f \gamma_p(R)}. \quad (17)$$

It should be noticed, that the effect of residual stress in the film is not taken into account in the present analysis, since yield strength is not affected significantly by isotropic stress.

3. Experimental procedures

Slide glass with a thickness of 1.2 mm ~ 1.5 mm and cover glass with a thickness of 0.12 mm ~ 0.17 mm were used as substrate material. Table 1 shows the chemical composition of the glass obtained by X-ray fluorescence analysis (Rigaku ZSX-100e). The Young's modulus and Poisson's ratio of these glasses are 71.3 GPa and 0.22, respectively. The thicker glass plates were used for the Vickers indentation with large loads, which formed cracks with radii larger than 50 μm. The glass plates were annealed at 723 K for 3.6 ks in order to remove pre-existing residual stresses. The films of 99.9% purity Au were deposited on the surfaces of these glass plates by using a DC sputtering machine (Eiko Engineering, IB-2). The film thickness was evaluated from the change in weight before and after the sputter-deposition, and the thickness of very thin films was measured by using atomic force microscopy. The film thickness ranged from 23 nm to 227 nm. The Vickers indentation was conducted at room temperature. The load changed from 1.96 N to 4.9 N for thinner glass substrates and from 1.96 N to 19.6 N for thicker glass substrates. The indentation tests were carried out twenty times for each load. The half-lengths of radial cracks which developed only in the diagonal directions of indent were measured by using an optical microscope (OM) and a field-emission scanning electron microscope (SEM, Hitachi S-4100H). The COD profiles of some cracks, in uncoated glass were also measured by the SEM.

Table 1. Chemical composition of glass substrate (mass%)

SiO_2	B_2O_3	Al_2O_3	Na_2O	K_2O	TiO_2	ZnO	P_2O_5	Fe_2O_3	Sb_2O_3
60.9	11.1	4.17	7.03	7.08	4.26	5.28	0.018	0.0176	0.0918

4. Results and discussion

4.1 Uncoated glass

Fig. 1 shows an example of radial cracks formed around the Vickers indent in uncoated glass. At light loads ranging from 0.98 N to 2.94 N, some cracks deviated from the diagonal directions of indent or very short cracks were formed in the diagonal direction, as is shown in this figure. These cracks were excluded in the measurement. The values of COD were measured in the direction normal to the crack propagation, as shown in Fig. 1(b). Fig. 2 shows typical examples of COD profiles measured at 2.94 N and 9.8 N. These COD profiles are similar in shape to those in soda-lime glass which were measured at the same load range by us, and those at larger loads (9.1 N - 98 N) by Burghard *et al* [14]. Solid curves in Fig. 2 are fitting curves which are obtained by applying Eq. (8) to the COD values in the range of $C/2 \le r \le C$. One can see that the solid curves agree fairly well with the measured COD profiles in this range. The values of δ_o estimated by the solid curves are 67.5 nm at 2.94 N and 92.7 nm at 9.8 N, providing 0.32 MPa·m$^{1/2}$ for the value of K_{tip} independently on the crack size or load. Broken curves in Fig. 2 are the COD profiles, which are obtained by inserting the values of δ_o into Eq. (2). The coincidence of the COD profiles predicted by Eq. (2) with the measured ones is limited to a distance of about 10% from the crack tips. As a result, the accurate determination of δ_o by using Eq. (2) is very difficult at small loads, since the measurement error as well as the scatter of COD become relatively large compared to the small COD values near the crack tips.

Table 2 shows the average values of d, C, H and K_C and γ_s in uncoated glass, where the surface energy of glass is given by $\gamma_s = K_C^2/(2E)$. All of the values of d and C listed in this table are measured by SEM observation. It should be noted here that the OM measurement yielded 6.4 GPa and 0.65 MPa·m$^{1/2}$ for H and K_C, respectively, as will be shown in Table 3. On the other hand, the SEM observations leads to slightly higher hardness and smaller fracture toughness compared to those measured by OM observation. It is considered that this discrepancy in H and K_C arises from the fact that SEM images do not have such a large sensitivity to the change in the height of surface

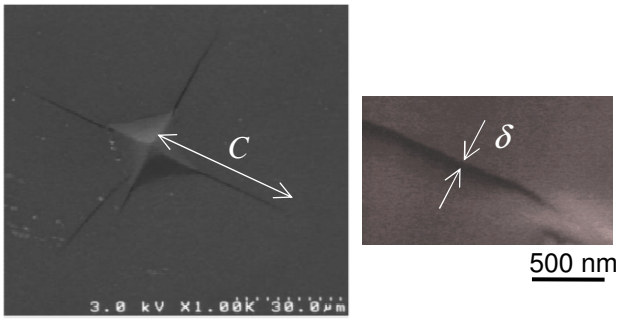

(a) Indent and radial cracks. (b) Crack tip.

Fig. 1. SEM photographs of radial cracks in uncoated glass (P = 2.94 N).

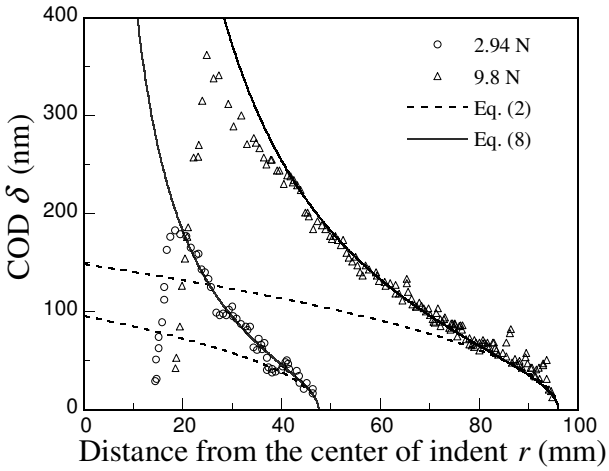

Fig. 2. COD profiles in uncoated glass at 2.94 N and 9.8 N.

Table 2. The values of d, C, H, K_C and γ_s evaluated by SEM observation.

P (N)	d (mm)	C (mm)	H (GPa)	K_C (MPa·m$^{1/2}$)	γ_s (J/m^2)
0.98	17.1	19.7	6.70	0.585	2.40
1.96	24.0	30.2	6.81	0.612	2.62
2.94	29.3	38.2	6.85	0.643	2.90
4.90	38.3	56.0	6.68	0.611	2.62

as OM images provides, while OM observation do not give as high a resolution in the measurement of crack size as that of SEM observation. In the evaluation of the mechanical properties of thin films, we will use the data measured by SEM observation in order to avoid the systematic error arising from a difference in measurement method.

4.2 Apparent hardness and apparent fracture toughness of Au/glasss

Fig. 3 shows the OM and SEM images of 23 nm thick Au/glass indented at a load of 2.94 N. The Au film is translucent to light at this thickness, so we can estimate the crack size in glass substrate underneath the film. Table 3 shows the values of d and C in uncoated glass and 23 nm thick Au/glass, which were measured by OM observation. It is obvious that the crack size is nearly equal between these specimens, while the indent size of the Au/glass is slightly larger than that of the uncoated glass. As a result, the apparent hardness, H_A, of the Au/glass is lowered slightly compared to that of the uncoated glass. The value of χ in the Au/glass increased only by 6.5% so that its apparent fracture toughness, K_A, is close to that of the uncoated glass. On the other hand, secondary electrons in SEM are emitted from a very shallow surface layer within a depth of a few nm. Accordingly we can observe the morphology of cracks formed only in the Au film. Fig. 3(c) shows the enlarged SEM micrograph of a crack front shown highlighted by the square in Fig. 3(b). One can see from this figure, that the crack front in the Au film has a faintly dark contrast; and its length is about 1.8 μm. Comparing this result with the crack size measured by OM observation, it is considered that the Au film is elongated over this distance from the crack front in the underlying substrate.
Fig. 4 shows the load-dependence of the hardness (H) of uncoated glass and the apparent hardness (H_A) of Au/glass. The apparent hardness decreases when increasing the thickness of Au film, and the difference between H and H_A tends to increase with lowering the load. The decrease in the apparent hardness of Au/glass is brought by the plastic deformation of the Au film, which is evidenced by the morphology of the indented surface of 227 nm thick Au/glass shown in Fig 5. When the film thickness is 227 μm, radial cracks were not observed at loads less than 9.8 N. The

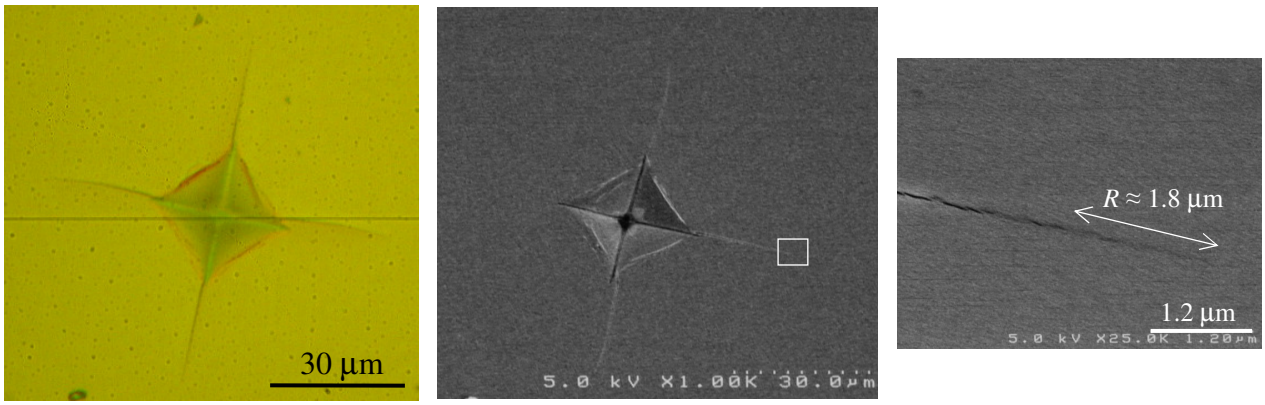

(a) OM photograph. (b) SEM micrograph. (c) SEM micrograph of crack front.

Fig. 3. Cracks formed around the Vickers indent in 23 nm thick Au/glass (P =2.94 N).

Table 3. The values of d, C, H, H_A, K_C and K_A evaluated by OM observation.

Crack system	d (μm)	C (μm)	H , H_A (GPa)	K_C, K_A (MPa·m$^{1/2}$)
Glass	29.2	38.2	6.38	0.645
23 nm thick Au/glass	31.2	38.7	5.62	0.675

maximum COD of uncoated glass is 182 nm at 2.94 N and 360 nm at 9.8 N (Fig. 2). Thus it is obvious that when the film thickness is larger than the maximum COD, cracks are not formed in the film. The apparent fracture toughness of Au/glass evaluated by using $\chi_A = 0.016(E/H_A)^{1/2}$ in Eq. (6) increased about twice at a thickness of 40 nm and about four times at 100 nm in comparison with the fracture toughness of uncoated glass.

4.3 Analysis of 34 nm thick Au/glass

As mentioned in sections 4.1 and 4.2, the COD profiles for $C/2 \le r \le C$ in uncoated glass obey those predicted by Eq. (8), and the Au/glass crack systems investigated here show their discontinuity at the film/substrate interfaces. As a case study, the mechanical properties of 34 nm thick Au film coated on glass substrate are evaluated here. The apparent hardness of the Au/glass decreases by about 0.5 GPa, but its apparent fracture toughness increases by a factor of about 1.8, in comparison with the hardness and fracture toughness of uncoated glass (Fig. 6). The value of R increases with load, and the ratio, R/C, is 30 - 35% irrespectively of load, as is shown in Fig. 7.

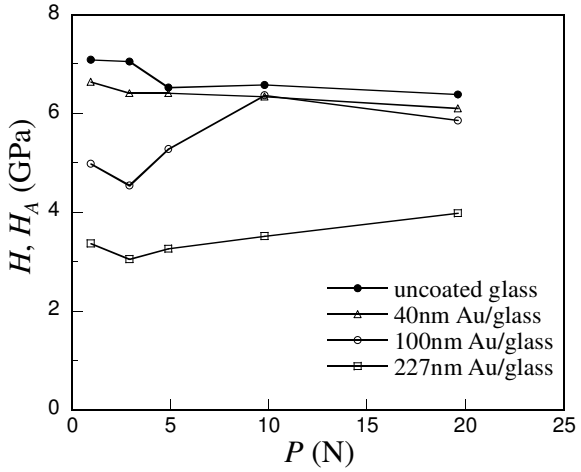

Fig. 4. Load-dependence of hardness in uncoated glass and Au/glass.

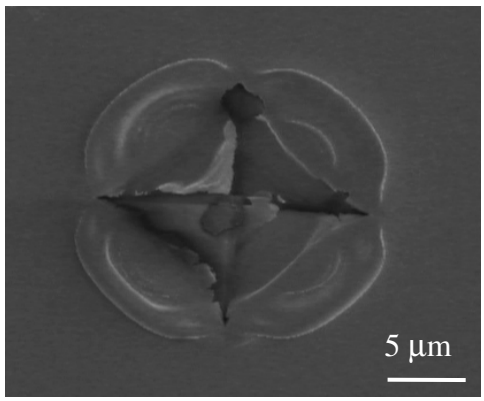

Fig. 5. Indent formed on 227 nm thick Au/glass (P = 2.94 N)

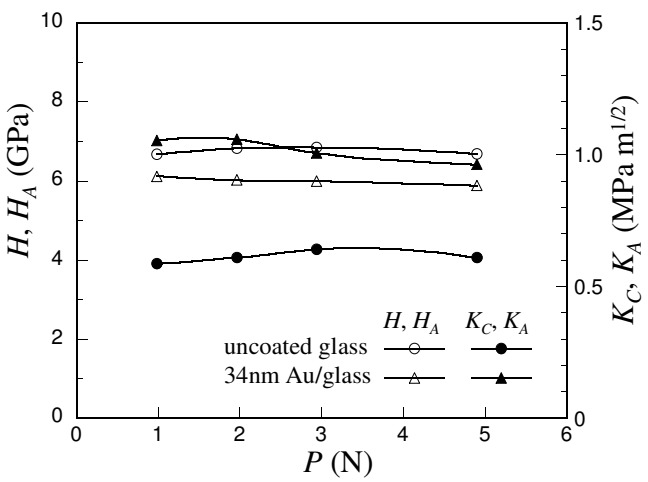

Fig. 6. Load-dependence of apparent hardness and fracture toughness in 34 nm thick Au/glass.

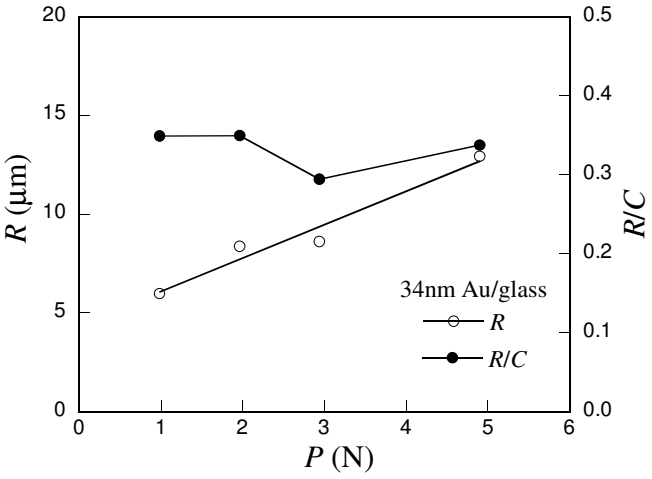

Fig. 7. Load-dependence of R and R/C in 34 nm thick Au/glass.

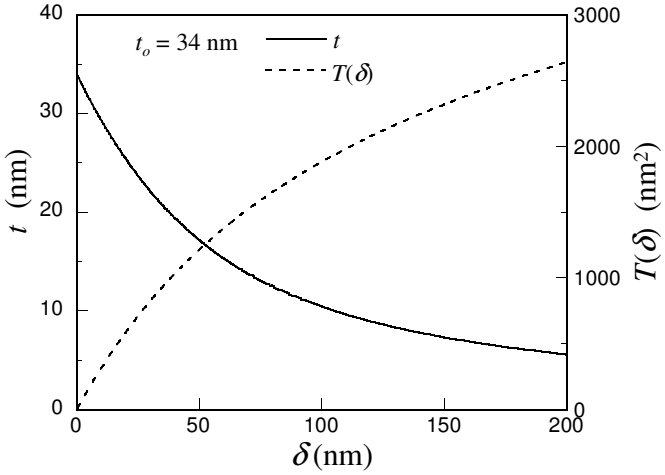

Fig. 8. The change in film thickness and $T(\delta)$ with COD in 34 nm thick Au film.

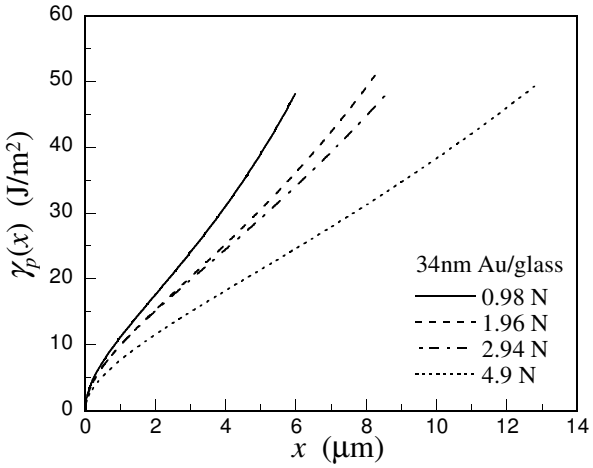

Fig. 9. The profiles of local plastic work per unit area in 34 nm thick Au film.

Table 4. Parameters and mechanical properties evaluated for 34 nm thick Au film.

P (N)	δ_o (nm)	R (μm)	$V(R)$ (x10^6 nm^3)	σ_y (MPa)	$\gamma_p(R)$ (J/m^2)	K_{fC} (MPa·m$^{1/2}$)
0.98	42.8	5.98	4.52	695	48.2	1.94
1.96	52.9	8.38	7.11	633	51.9	2.01
2.94	59.6	8.62	7.17	639	48.4	1.94
4.9	72.1	12.93	12.58	499	49.9	1.97

Therefore we can use Eq. (8) to estimate the COD profile in the substrate. Fig. 8 shows the changes of t and $T(\delta)$ as a function of δ, which are calculated by inserting Eq. (8) into Eq. (10) and Eq. (13) and using the value of δ_o determined by K_{tip} = 0.32 MPa·m$^{1/2}$.

The values of σ_y at 0.98 N - 4.9 N obtained by setting the Young's modulus of Au as 78 GPa [20] are listed with other parameters in Table 4. The average yield strength of 34 nm thick Au film evaluated in the present study is 620 MPa, which is comparable with about 400 MPa in 2.7 μm thick Au film [21] and about 600 - 900 MPa in 0.85 μm and 1.76 μm thick Au films [22]. However, it has been shown that the mechanical properties of thin Au films depend on the thickness [22, 23], temperature [21, 22] and strain rate [22]. One of the most available data to be compared with the present result may be the mechanical properties of 20 nm thick Au films examined by Olliges *et al* [24]. They elongated such very thin Au films deposited on polyimide substrates and measured the stress in the films by using synchrotron X-ray. They reported that the yield strength of the films ranged from 700 MPa to 875 MPa at room temperature, which is in a good accordance with the yield strength obtained for 34 nm thick Au film. The local plastic energy $\gamma_p(x)$ of 34 nm thick Au film increases with the distance from crack tip and its shape resembles the COD profile near the crack tip, as is shown in Fig. 9. The maximum value of COD, however, does not depend on the value of R or load. Consequently the maximum plastic work and fracture toughness of the Au film is about 50 J/m^2 and 2.0 MPa·m$^{1/2}$, respectively (Table 4).

5. Summary

In the present study, microcracking induced by the Vickers indentation was applied to the evaluation of the mechanical properties of very thin films of ductile metals. For this purpose, a simple expression was proposed for the estimation of the COD of radial cracks in brittle substrates, which agreed very well with the COD profiles measured in uncoated glass in the range of $C/2 \le r \le C$. The

comparison of the OM and SEM images of 23 nm thick Au/glass crack fronts clearly showed that the film was elongated to failure at the crack mouth of the substrate. However, when the film thickness exceeded the COD of the substrate, radial cracks were not formed in the film. These results suggest the validity of assumptions used in the present analysis of the mechanical properties of very thin metallic films. The yield strength of 34 nm thick Au film was evaluated to be about 620 MPa, which is comparable with the yield strength of very thin Au films given in literature. The maximum plastic work and fracture toughness of 34 nm thick Au film were also evaluated to be 50 J/m^2 and 2.0 $MPam^{1/2}$, respectively.

Acknowledgement

We thank the staff of Division of Intrumental Analysis, NSCRE, Kagoshima University for their great help.

References

[1] D. Tabor, Hardness of Metals, Oxford University Press, New York, 2000.
[2] G. Dieter, Mechanical Metallurgy, 3rd Ed., McGraw-Hill, New York, 1986.
[3] A.E.H. Love, Quat J Math, 10 (1939) 161−175.
[4] W.C. Oliver, G.M. Pharr, J Mater Res, 7 (1992) 1564−1583.
[5] R. Hill, The Mathematical Theory of Plasticity, Oxford University Press, Oxford, 1950.
[6] K.L. Johnson, Contact Mechanics, Cambridge University Press, Cambridge, 1985.
[7] S.M. Han, R. Saha, D. Nix, Acta Mater, 54 (2006) 1571−1581.
[8] M. Dietiker, R.D. Nyilas, C. Solenthaler, R. Spolenak, Acta Mater, 56 (2008) 3887−3899.
[9] B.R. Lawn, Fracture of Brittle Materials, 2nd Ed., Cambridge University Press, Cambridge, 1993.
[10] T. Fett, Report FZKA 6757, Forschungszentrum Karlsruhe, Karlsruhe, 2002.
[11] Z. Burghard, A. Zimmermann, J. Rödel, F. Aldinger, B.R. Lawn, Acta Mater, 52 (2004) 293−297.
[12] T. Fett, G. Rizzi, Report FZKA 6907, Forschungszentrum Karlsruhe, Karlsruhe, 2003.
[13] B.R. Lawn and A.G. Evans, J Mater Sci, 12 (1977) 2195−2199.
[14] D.B. Marshall and B.R. Lawn, J Mater Sci, 14 2001 (1979).
[15] H. Tada, P.C. Paris, G.R. Irwin, The Stress Analysis of Cracks Handbook, 3rd Ed., ASME, 2000.
[16] I.J. McColm, Ceramic Hardness, Prenum Press, New York, 2010.
[17] G.R. Anstis, P. Chantikul, D.B. Marshall and B.R. Lawn, J Am Ceram Soc, 64 533 (1981).
[18] H. Miyamoto, Three Dimensional Elasticity, Shokabo, Tokyo, 1967 (in Japanese).
[19] I.S. Gradshteyn, I.M. Ryzhik, Tables of Integrals, Series, and Products 5th Ed., Academic Press, San Diego, 1994.
[20] T.H. Courtney, Mechanical Behavior of Materials, McGraw-Hill, New York, 1990.
[21] A.A. Volinsky, N.R. Moody, W.W. Gerberich, J Mater Res, 19 (2004) 2650−2657.
[22] K. Jonnalagadda, N. Karanjgaokar, I. Chasiotis, J. Chee, D. Peroulis, Acta Mater, 58 (2010) 4674−4684.
[23] H.D. Espinosa, B.C. Prorok, B. Peng, J Mech Phys Sol, 52 (2004) 667−689.
[24] S. Olliges, S. Frank, P.A. Gruber, V. Auzelyte, H. Solak, R. Spolenak, Mater Sci Eng A, 528 (2011) 6203−6209.